

# Anisotropic mass ejection in binary mergers

T. Morris<sup>1,2★</sup> and Ph. Podsiadlowski<sup>1</sup>

<sup>1</sup>*Department of Astrophysics, University of Oxford, Keble Road, Oxford OX1 3RH*

<sup>2</sup>*Max-Planck Institut für Astrophysik, Karl-Schwarzschild-Str. 1, 85741 Garching, Germany*

Accepted 2005 September 23. Received 2005 September 7; in original form 2005 February 15

## ABSTRACT

We investigate the mass loss from a rotationally distorted envelope following the early, rapid in-spiral of a companion star inside a common envelope. For initially wide, massive binaries ( $M_1 + M_2 = 20 M_\odot$ ,  $P \sim 10$  yr), the primary has a convective envelope at the onset of mass transfer and is able to store much of the available orbital angular momentum in its expanded envelope. Three-dimensional smoothed particle hydrodynamics calculations show that mass loss is enhanced at mid-latitudes due to shock reflection from a torus-shaped outer envelope. Mass ejection in the equatorial plane is completely suppressed if the shock wave is too weak to penetrate the outer envelope in the equatorial direction (typically when the energy deposited in the star is less than about one-third of the binding energy of the envelope). We present a parameter study to show how the geometry of the ejecta depends on the angular momentum and the energy deposited in the envelope during a merging event. Applications to the nearly axisymmetric, but very non-spherical nebulae around SN 1987A and Sheridan 25 are discussed, as well as possible links to RY Scuti and the Small Magellanic Cloud object R4.

**Key words:** hydrodynamics – binaries: close – circumstellar matter – supernovae: individual: SN 1987A.

## 1 INTRODUCTION

The common-envelope (CE) phase is one of the most important and least understood phases of stellar evolution. Originally proposed by Paczyński (1976) to explain the origin of short-period binaries with compact objects, it can also significantly alter the evolution of systems in which the envelope remains bound, leaving an atypical single star (see e.g. Ivanova & Podsiadlowski 2003). For example, it is now widely believed that the unusual properties of the progenitor of SN 1987A are due to a binary merger some 20 000 yr before the explosion (Podsiadlowski & Ivanova 2003).

In this paper, we are interested in the case where the primary initiates mass transfer either when crossing the Hertzsprung gap (so-called early Case B mass transfer) or later as a red supergiant (late Case B/C mass transfer). In the latter case, the primary has already developed a deep convective envelope and mass transfer is dynamically unstable if the mass ratio exceeds a critical value, leading to a CE and spiral-in phase.

Early Case B mass transfer initially occurs on the thermal time-scale of the mass donor and is dynamically stable; but the secondary may not be able to accrete all of the transferred mass, and this may also lead to a CE system and possibly the merging of the system (e.g. Pols 1994; Wellstein, Langer & Braun 2001).

While the CE maintains co-rotation with the embedded binary, orbital angular momentum is efficiently transferred from the binary orbit to the envelope, where most of the initial orbital angular

momentum is stored:

$$L_{\text{orb}} = 6.60 \times 10^{54} \text{ g cm}^2 \text{ s}^{-1} A_{2500}^{1/2} M_{15} M_5 M_{20}^{-1/2}, \quad (1)$$

where  $A_{2500}$  is the orbital separation in units of  $2500 R_\odot$ ,  $M_{15}$  and  $M_5$  are the masses of the primary and the secondary in units of 15 and  $5 M_\odot$  (as indicated by the subscripts), respectively, and  $M_{20} = M_1 + M_2$  is the total mass in units of  $20 M_\odot$ . This phase may last perhaps for a few decades and ends when the envelope becomes differentially rotating. The subsequent rapid plunge-in of the secondary then drives significant envelope expansion and the ejection of at least some of the envelope (Meyer & Meyer-Hofmeister 1979; Sandquist et al. 1998; Taam & Sandquist 2000; Podsiadlowski 2001; Ivanova & Podsiadlowski 2003). If the envelope is not completely ejected in this phase (the case of interest in this study), the spiral-in continues and now becomes self-regulated where all the energy dissipated by the further orbital decay is transported to the surface and radiated away (Meyer & Meyer-Hofmeister 1979; Podsiadlowski 2001). A second phase of mass loss may result from a nuclear flash that may occur during the final core merger (Ivanova & Podsiadlowski 2003).

Previous one-dimensional numerical simulations by Podsiadlowski (2001) have shown that significant mass loss may occur even when most of the envelope remains bound. In the three-dimensional models of Livio & Soker (1988) and Sandquist et al. (1998), most mass loss occurs in the orbital plane of the binary. However, these authors considered the case where most/all of the envelope was ejected. In this study, we consider the less energetic case appropriate for a merger. As we will show, in this case mass loss

★E-mail: tsm@mpa-garching.mpg.de

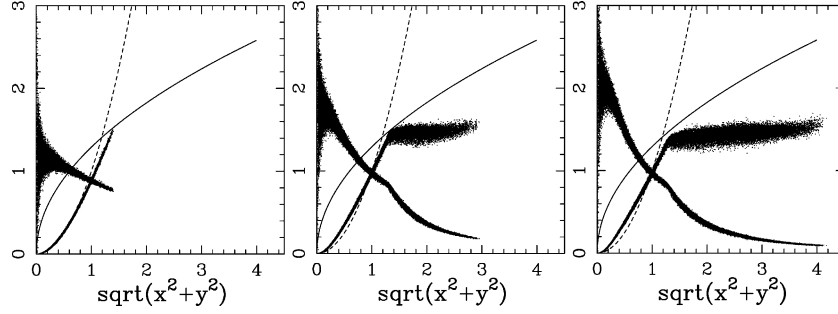


**Figure 1.** Particle plots showing specific angular momentum (increasing outwards) and angular velocity for the three cases of angular momentum  $L = 0.235, 0.588$  and  $0.817\sqrt{GM^3R}$  from left-hand panel to right-hand panel. The solid curves give the critical specific angular momentum  $j_c = \sqrt{G(5M/3)R}$  while the dashed curves show the solid-body profiles  $j = \omega r^2$  where  $\omega = 1$ . All quantities are given in code units.

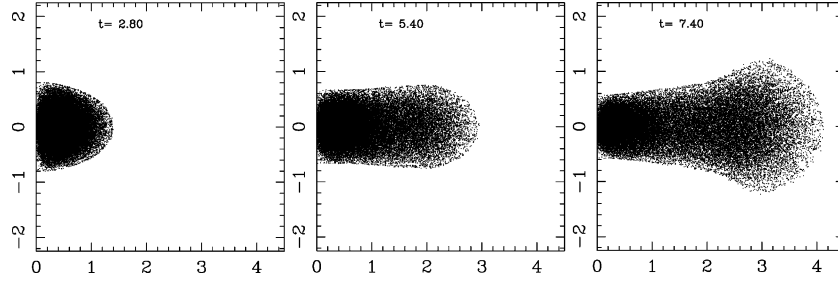


**Figure 2.** Distribution of SPH particles in the meridional plane immediately after the spin-up for the three cases of angular momentum  $L = 0.235, 0.588$  and  $0.817\sqrt{GM^3R}$  from left-hand panel to right-hand panel. For other properties see Table 1.

may preferentially occur at mid-latitudes and be suppressed in the equatorial direction if the energy deposited is less than about one-third of the binding energy of the envelope. In Section 2, we outline our numerical method and in Section 3 we present the main results of our study and their dependence on the input parameters. In Section 4, we apply these results to observed systems, in particular SN 1987A and Sheridan 25.

## 2 NUMERICAL METHOD

We model the CE as a condensed polytrope with adiabatic index  $\gamma = 5/3$  with a central point mass which contains two-fifths of the system mass.<sup>1</sup> Assuming spherical symmetry and hydrostatic equilibrium initially, we obtain the radial density profile by integrating the dimensionless equations,

$$\frac{d\bar{\rho}}{d\bar{z}} = -A \frac{\bar{m}}{z^2} \bar{\rho}^{2-\gamma} = \left( \frac{G}{\gamma K} \frac{M_{\text{core}}^{2-\gamma}}{R_{\text{core}}^{4-3\gamma}} \right) \frac{\bar{m}}{z^2} \bar{\rho}^{2-\gamma}, \quad (2)$$

$$\frac{d\bar{m}}{d\bar{z}} = 4\pi z^2 \bar{\rho} \quad (3)$$

with the inner boundary conditions

$$\bar{m}(z = 1) = 1 \quad (4)$$

and

$$\bar{\rho}(z = 1) = (\gamma A)^{1/\gamma} \left[ \frac{3(\delta - 1)}{8\pi} \right]^{1/\gamma}, \quad (5)$$

where  $z = r/R_{\text{core}}$ ,  $\bar{m} = M(r)/M_{\text{core}}$  and  $\rho = \bar{\rho}M_{\text{core}}/R_{\text{core}}^3$ . The free parameters  $A$  and  $\delta$  are determined from the surface boundary conditions  $\bar{\rho}(z = Z) = 0$  and  $\bar{m}(z = Z) = M_{\text{core}}/M_{\text{core}}$  where  $Z =$

<sup>1</sup> These parameters were chosen to roughly represent the inferred properties during the late spiral-in phase for merger models of SN 1987A, where the core fraction represents the immersed binary core, consisting of the core of the primary and the spiraling-in companion.

$R_{\text{core}}/R_{\text{core}}$ . For all hydrodynamical simulations presented in this paper, we use the GADGET code of Springel, Yoshida & White (2001), which implements gravity and gas dynamics using the smoothed particle hydrodynamics (SPH) method (Monaghan 1992). The envelope density is sampled with  $10^5$  particles using a Monte Carlo method followed by isentropic relaxation to reduce numerical noise (Lucy 1977). The code units are  $M$ , the mass of the envelope and  $R$ , the initial (non-rotating) stellar radius (the total stellar mass including the core is  $5M/3$ ). This implies that time is measured in the code in units of  $\sqrt{R^3/GM}$  and velocity in units of  $\sqrt{GM/R}$ . Note that this allows simple re-scaling of the results presented in this paper.

To parametrize the spin-up of the envelope and the energy deposited by the spiral-in, we define two parameters  $\alpha$  and  $\beta$ , where  $\alpha \equiv \Delta E/E_B$  is the ratio of the energy deposited to the binding energy of the envelope and  $\beta \equiv L/\sqrt{GM^3R}$  is a dimensionless measure of the envelope angular momentum following the early in-spiral of the secondary.

To spin up the envelope we add angular momentum on a dynamical time-scale using the following recipe: during every fixed time-step  $\Delta t = 0.025$ , the rotational velocity of each particle is incremented by an amount

$$\Delta v_i = r_i \Delta \Omega, \quad \text{provided } v_i < \sqrt{-\phi_i}, \quad (6)$$

that is, as long as the velocity remains sub-Keplerian. The angular velocity increment is  $\Delta \Omega = 0.0093$  of the critical velocity at the surface of the non-rotating envelope ( $r = 1$  in code units). If at any time the particle velocity  $v_i$  reaches the local Keplerian velocity, we set  $\Delta v_i = 0$  thereafter. This leads to solid-body rotation in the inner envelope and a slightly rising specific angular momentum profile in the outer envelope (see Fig. 1). The spin-up phase is terminated when  $\beta$  reaches 0.235, 0.588 and 0.817, respectively, for the three cases we consider in this paper (note that no particles become super-critical; see Fig. 2 and Table 1). These three values correspond to

**Table 1.** Properties of the three rotating envelopes immediately before the energy deposition for the zero-delay case. All values in CGS units are for  $M_{\text{env}} = 12 M_{\odot}$ ,  $R = 1500 R_{\odot}$  appropriate to the merger model for SN 1987A.

$T/W$	0.039	0.117	0.151
$\beta = L/\sqrt{GM^3R}$	0.235	0.588	0.817
Angular momentum ( $10^{54} \text{ g cm}^2 \text{ s}^{-1}$ )	2.3	5.7	8.0
Mean angular velocity ( $10^{-8} \text{ s}^{-1}$ )	3.7	2.2	1.1
Flattening $R_{\text{eq}}/R_{\text{polar}}$	1.7	4.3	6.8
Rotation velocity ( $\text{km s}^{-1}$ )	42	21	15
Fraction of critical rotation	0.96	0.69	0.61
Binding energy ( $10^{47} \text{ erg}$ )	-6.2	-5.4	-4.5

**Table 2.** Properties of the rotating envelopes immediately before the energy deposition, for  $L = 0.588\sqrt{GM^3R}$  (top) and  $L = 0.817\sqrt{GM^3R}$  (below) and for three values of the time delay following the spin-up of the envelope.

$t_{\text{delay}}$ (yr)	0.67	1.35	2.69
$T/W$	0.090	0.078	0.071
Angular momentum ( $10^{54} \text{ g cm}^2 \text{ s}^{-1}$ )	5.7	5.7	5.7
Mean angular velocity ( $10^{-8} \text{ s}^{-1}$ )	1.46	1.07	0.71
Flattening $R_{\text{eq}}/R_{\text{polar}}$	5.2	5.4	7.0
Rotation velocity ( $\text{km s}^{-1}$ )	18	16	13
Fraction of critical rotation	0.67	0.63	0.57
Binding energy ( $10^{47} \text{ erg}$ )	-5.2	-5.1	-5.0
$T/W$	0.121	0.104	0.088
Angular momentum ( $10^{54} \text{ g cm}^2 \text{ s}^{-1}$ )	8.0	8.0	8.0
Mean angular velocity ( $10^{-8} \text{ s}^{-1}$ )	0.79	0.61	0.42
Flattening $R_{\text{eq}}/R_{\text{polar}}$	7.5	8.3	9.6
Rotation velocity ( $\text{km s}^{-1}$ )	14	13	11
Fraction of critical rotation	0.58	0.56	0.52
Binding energy ( $10^{47} \text{ erg}$ )	-4.3	-4.2	-4.1

envelope angular momenta of 2.3, 5.7 and  $8.0 \times 10^{54} \text{ g cm}^2 \text{ s}^{-1}$  which is comparable to the available orbital angular momentum (equation 1).

To simulate the deposition of the energy and the rapid heating of the envelope during the plunge-in phase, we then add entropy to the inner envelope [ $r < 2/15R$ , from calculations discussed in Ivanova & Podsiadlowski (2003) and Podsiadlowski (2001)]. Initially, we consider the case where the energy is deposited immediately after the envelope has been spun up. The response of the envelope is then followed for 10–15 dynamical time-scales after the instantaneous energy deposition, at which point all the ejected particles are to good approximation on ballistic trajectories.

Since we do not follow the evolution of the spiraling-in binary components, we do not encounter resolution problems when the orbital separation becomes comparable to the SPH smoothing length

**Table 3.** Total mass ejected at  $t = 10t_{\text{dyn}} \simeq 8.2 \text{ yr}$  after the entropy deposition in the inner envelope, in solar masses.  $T$  is the time delay in yr following the spin-up phase.

$\alpha = \frac{E}{E_{\text{BE}}}$	$\beta = \frac{L}{\sqrt{GM^3R}} = 0.235$ $T = 0$	$\beta = 0.588$			$\beta = 0.817$				
		$T = 0$	$T = 0.67$	$T = 1.35$	$T = 2.69$	$T = 0$	$T = 0.67$	$T = 1.35$	$T = 2.69$
0.25	0.24	0.17	0.14	0.17	0.21	0.18	0.15	0.16	0.18
0.33	0.44	0.55	0.32	0.36	0.42	0.34	0.32	0.34	0.38
0.4	0.83	1.12	0.51	0.55	0.63	0.68	0.49	0.51	0.58
0.5	1.33	2.15	1.10	0.91	1.00	1.67	0.79	0.81	0.89

(Livio & Soker 1988); our model is mainly limited by physical approximations (such as the equation of state; the lack of energy transport) rather than the numerical resolution (see Appendix A) – except near the surface. The steep density profile at the surface is poorly resolved by SPH particles, and a well-known problem of SPH models in this context (as, e.g. seen in supernova models) is an over-estimate of the mass contained in low-velocity material.

### 3 RESULTS AND DISCUSSION

As shown in Fig. 2, the addition of substantial angular momentum strongly distorts the envelope (see, in particular, the  $8 \times 10^{54} \text{ g cm}^2 \text{ s}^{-1}$  calculation and Table 1). These profiles are similar to the  $(n, n') = (1.5, 0)$  sequence of inviscid polytropic models calculated in Bodenheimer & Ostriker (1973), although our envelopes are more extended for a given value of  $T/W$  (the ratio of kinetic to potential energy) due to some viscous heating. The outer envelopes contain 1.7 and  $4M_{\odot}$  for  $\beta = 0.588$  and 0.817, respectively, and both have a temperature of  $\sim 10^4 \text{ K}$ .

Following the energy deposition, matter is ejected in a very anisotropic way depending on the rotational distortion and the amount of energy deposited (i.e. depends on  $\alpha$  and  $\beta$ ; see Fig. 3). Generally envelope material is first ejected (i.e. reaches escape speed) in the polar direction. At low rotation ( $\beta = 0.235$ , not illustrated) mass is also ejected in the equatorial plane at early times, and the distribution is more or less spherically symmetric. For larger values of  $\beta$ , envelope ejection in the equatorial plane is suppressed for low values of  $\alpha$  or enhanced for large values of  $\alpha$ . In particular, no mass is lost in the equatorial plane if the energy fraction  $\alpha$  is less than some critical value  $\alpha_c$  which increases with increasing  $\beta$ . If no matter is ejected in the equatorial plane, we find a strong mass excess at mid-latitudes due to shock focusing by the extended envelope (as discussed further below).

In Sections 3.1 and 3.2, we discuss two typical calculations with  $\alpha = 0.33$ ,  $\beta = 0.82$  and  $\alpha = 0.35$ ,  $\beta = 0.66$ , respectively. In the  $\beta = 0.82$  case, the critical energy fraction is  $\alpha_c = 0.39$  (from Fig. 4), and therefore no material is ejected in the equatorial plane. In both these calculations energy is deposited immediately after the spin-up phase.

In Section 3.3, we discuss the mass-loss geometry due to a variation of  $\alpha$  and  $\beta$  for different time delays between the spin-up and energy-deposition phase (no time delay and a delay of 1.35 yr, respectively; see also Table 2). The dynamical time delay is a free parameter in our model which could be constrained by more detailed models that follow the spiral-in explicitly.

#### 3.1 Model 1: $\alpha = 0.33, \beta = 0.817$

In this model, the envelope is significantly distorted by the rotation (column 3 of Table 1), and most mass is ejected at a latitude between  $30^\circ$  and  $40^\circ$ . Despite the reduction in the effective gravity

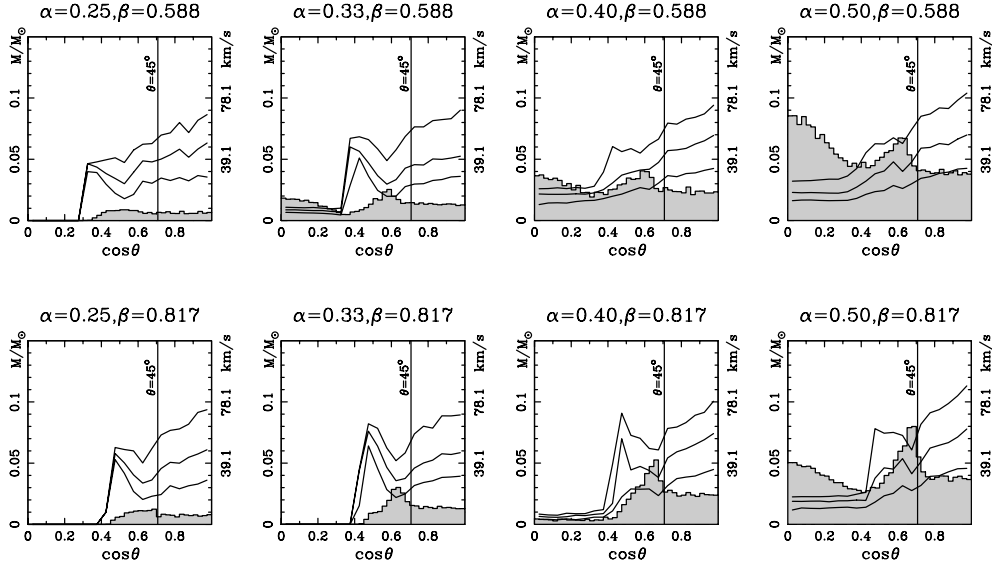


**Figure 3.** The final amount of mass ejected (left-hand scale) as a function of  $\cos\theta$  where  $\theta$  is the polar angle for different values of the energy deposition and different values of the angular momentum of the envelope (the values of  $\alpha$  and  $\beta$  are given above each panel;  $\alpha = 1$  corresponds to an energy of  $5.4 \times 10^{47}$  erg (for  $\beta = 0.588$ ) and  $4.5 \times 10^{47}$  erg (for  $\beta = 0.817$ ) while  $\beta = 1$  corresponds to an angular momentum  $L_{\text{env}} = 9.7 \times 10^{54}$  g cm<sup>2</sup> s<sup>-1</sup>. The central solid curves show the median velocity of the material (right-hand scale) ejected as a function of polar angle, and the upper and lower curves give the range of velocities that includes 50 per cent of the material.

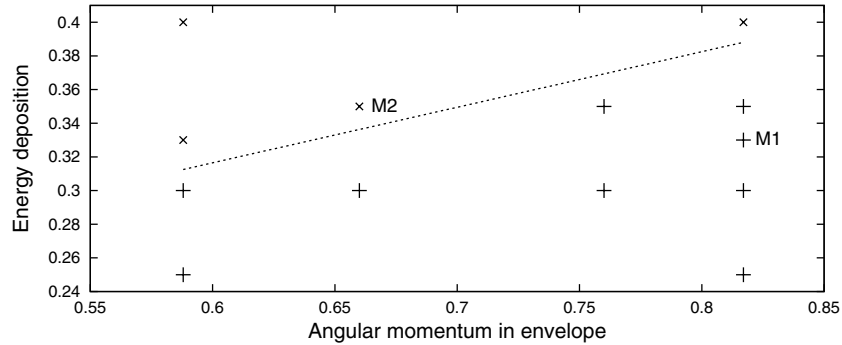


**Figure 4.** The  $(\beta, \alpha)$  plane at  $t = 10$ , for the zero-delay case. The line separates models with (above) and without (below) equatorial mass ejection. Labelled models correspond to Models 1 and 2 discussed in the text.

close to the equator, very little mass is ejected there. The absence of ejected material in the equatorial plane is relatively easy to understand from the strong rotational deformation, since the shock wave cannot penetrate the outer envelope in the equatorial direction.

However, it is not quite so obvious how the mass enhancement at mid-latitudes arises. To illustrate the origin of this enhancement, we plot in Fig. 5 the evolution of the angular momentum in the  $z$ -direction relative to the total angular momentum for selected particles, which eventually escape, as a function of distance from the rotation axis during the early ejection phase. The ratio  $L_z/L$  parametrizes the inclination of the orbit of a particle, and its change shows the effects of the strong pressure gradients that act during this phase. Particles initially ejected at mid-latitudes move poleward shortly after ejection, reach a minimum in  $L_z/L$  before  $t = 3$  (e.g. the blue trajectory in Fig. 5 which reaches a minimum at  $L_z/L = 0.5$ ) and then evolve towards a ballistic orbit with a lower inclination.

During the strong poleward deflection at  $t = 2$ , a bow shock forms ahead of the massive outer envelope (see Fig. 6), which deflects particles away from the equatorial plane. Hence, the mass loss pole-

ward of  $\theta = 30^\circ$  changes from isotropic at  $t = 2$  to strongly peaked at  $t = 3$ , where  $\theta$  is the co-latitude.

The second deviation in Fig. 5 can be understood by the reflection of particles from slow-moving material at higher latitudes, which was ejected slightly earlier. This leads to a compression of the outflow at mid-latitudes ( $L_z/L \sim 0.65$ ), increasing the density enhancement. After  $t = 5$  the particles follow nearly radial trajectories, although the trajectories are not yet quite ballistic. By  $t = 10$  the flow is almost completely ballistic (as indicated by the fact that  $L_z/L$  remains constant thereafter).

### 3.2 Model 2: $\alpha = 0.35, \beta = 0.66$

The principal effect of the reduced angular momentum of the envelope is that the shock wave eventually reaches the surface in the equatorial region, and that some material is ejected there at low velocities (similar to the  $\alpha = 0.33$  and  $\beta = 0.588$  model in Fig. 3 but with a larger excess at mid-latitudes). The total ejected mass at  $t = 10$  is  $0.51 M_\odot$ , of which  $0.04 M_\odot$  is ejected per unit solid angle in the equatorial plane, a value that is close to the value one would

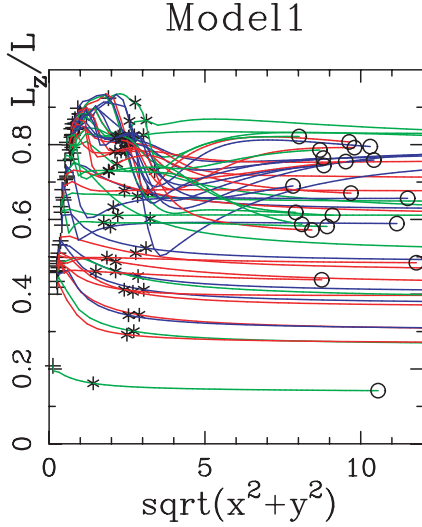


**Figure 5.**  $L_z/L$  as a function of distance from the rotation axis for selected (ejected) particles in Model 1 to illustrate the deviations from ballistic motion, where  $L_z$  is the angular momentum in the  $z$ -direction and  $L$  is the total angular momentum of the particle. Stars and circles show particle positions at  $t = 2$  and  $t = 15$  (in code units), respectively. The vertical axis shows  $L_z/L$ ; equatorial orbits are close to the top of the figure.

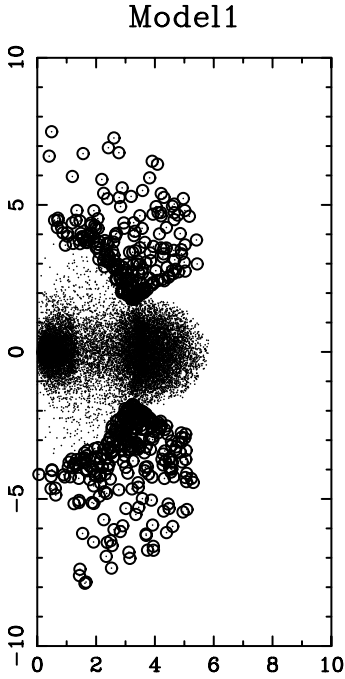


**Figure 6.** Particle snapshot at  $t = 3$  showing the deflection of the ejected particles (circled) from the outer envelope.

expect if the ejected mass had spherical symmetry. Initially, the flow is compressed due to the Bjorkman–Cassinelli effect (Bjorkman & Cassinelli 1993), but a strong density enhancement of one to two orders of magnitude does not form due to the fact that our envelope is extended and mainly supported by thermal pressure.

The mid-latitude enhancement contains a similar amount of mass as Model 1 discussed above, although its latitude is closer to the equator. As can be seen in Fig. 7, the flow is qualitatively similar to Model 1 (Fig. 5), but the shock interactions occur at lower latitudes since the star is less rotationally flattened. The velocity profile is

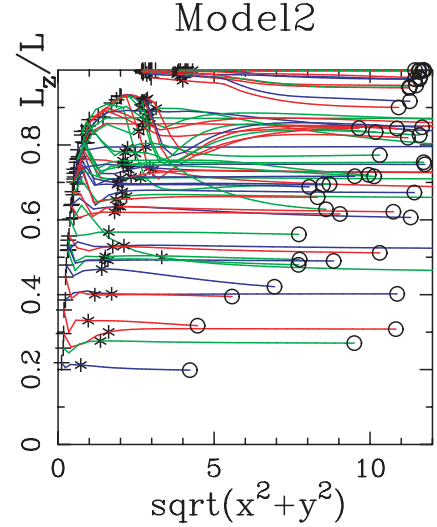


**Figure 7.** Similar to Fig. 5 for Model 2. Stars and circles show particle positions at  $t = 2$  and  $t = 15$  (in code units), respectively. The vertical axis is  $L_z/L$ .

similar in the polar region, since almost the same amount of energy was deposited in the envelope.

As in Model 1, the initial polar enhancement is caused by the absence of ejected matter elsewhere at early times. This leads to a large asphericity factor as a result of the small solid angle into which mass is ejected. Once mass has been ejected at lower latitudes, the ‘enhancement’ disappears.

### 3.3 Parameter study

In general, the mass ejected depends on three principal parameters: the amount of energy deposited ( $\Delta E$ ), the total angular momentum in the envelope ( $L$ ) and the time delay between the spin-up of the envelope and the deposition of the energy ( $t_{\text{delay}}$ ), which depends on the time-scale of the initial spiral-in phase. Variation of these parameters leads to changes in (i) the total ejected mass, (ii) the presence or absence of ejected material in the equatorial plane, and (iii) the strength of the enhancement at mid-latitudes. The peak mass flux also moves to slightly higher latitudes with increasing rotation.

In Fig. 3, we show the results of a systematic parameter study. Each panel shows the geometry of the ejected mass as a function of  $\cos \theta$ , where  $\theta$  is the polar angle, once the ejecta are expanding ballistically on radial trajectories. The histograms show the mass ejected divided into bins of constant  $d \cos \theta$  (each bin subtends  $\pi/10$  sr), and the individual curves show the velocity distribution at each angle (the central curve gives the median velocity, and the upper and lower curves give the velocity range which includes 50 per cent of the ejected matter). The velocity and angular momentum scale according to

$$v_{\text{cr}} \sim 39 \text{ km s}^{-1} \left( \frac{M}{12 M_{\odot}} \frac{1500 R_{\odot}}{R} \right)^{1/2}, \quad (7)$$

and

$$L_{\text{env}} = \beta 9.7 \times 10^{54} \text{ g cm}^2 \text{ s}^{-1} \left( \frac{M}{12 M_{\odot}} \right)^{3/2} \left( \frac{R}{1500 R_{\odot}} \right)^{1/2}. \quad (8)$$

The peak at mid-latitudes, which is only present for sufficiently distorted envelopes with  $\beta > 0.5$ , remains up to  $\alpha = 1$ . The mass excess at mid-latitudes becomes more pronounced as the angular momentum increases. The velocity of the equatorial material, when

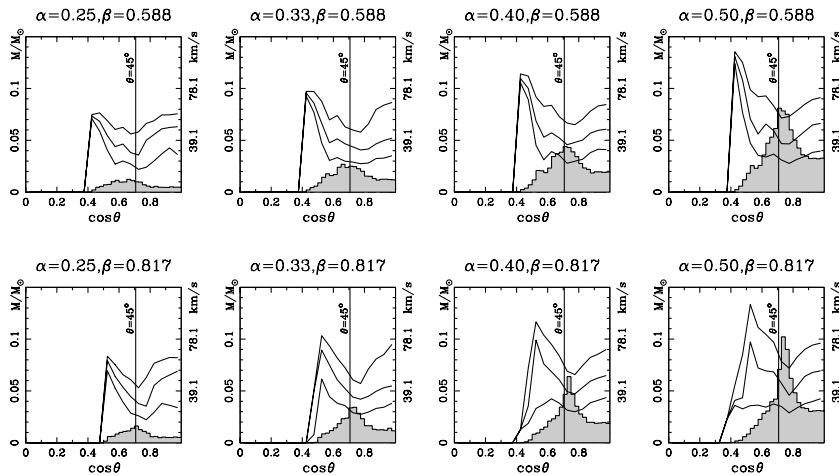


**Figure 8.** Properties of the ejected matter, similar to Fig. 3, for the case where the energy is deposited 1.35 yr (1.6 dynamical time-scales) after the spin-up of the envelope.

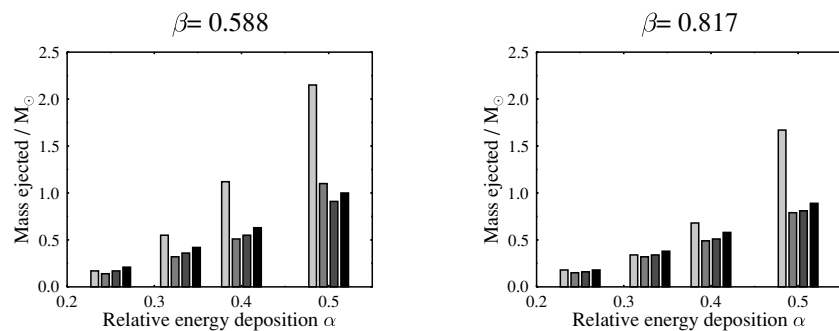


**Figure 9.** Total ejected mass for the calculations listed in Table 3 after  $\approx 8.2$  yr. Darker shading corresponds to longer delay times.

present, is typically a factor of 3–5 lower than the velocities at mid-latitudes, though this difference is reduced as the deposited energy is increased. The critical  $\alpha$  below which no mass is lost in the equatorial plane increases with rotation rate (see Fig. 4), since the envelope is more extended.

The trends remain very similar, when we introduce a time delay between the spin-up phase and the energy-deposition phase (see Fig. 8), except that the loss of material in the equatorial plane is now further impeded by the massive extended envelope, and the mid-latitude enhancement may be much stronger (see, e.g. the  $\alpha = 0.5$ ,  $\beta = 0.817$ ,  $t_{\text{delay}} = 1.35$  yr case). The peak has moved to slightly higher latitudes compared to the zero-delay case, but this is a small effect. During the time delay the outer envelope expands by a factor of  $\sim 1.5$  with a corresponding increase in the critical energy for equatorial mass ejection. Hence, increasing the energy drives more mass from each surface element but has little effect on the geometry. The total mass ejected for each value of the energy deposition  $\alpha$  and time delay is shown in Table 3 and Fig. 9.

### 3.4 Summary

Mass ejection during a CE phase leading to the complete merger of a binary system preferentially occurs at mid-latitudes due to shock reflection from an outer envelope containing a significant fraction of the initial orbital angular momentum. If the energy deposited is less than about one-third of the binding energy of the envelope no material is lost in the equatorial plane, in contrast to earlier models

which considered the higher-energy case appropriate for CE ejection (Livio & Soker 1988; Sandquist et al. 1998).

Although our results cannot be directly compared to those of Sandquist et al. (1998) since we do not model the in-spiral of the secondary, a number of similarities are apparent. The peak energy dissipation occurs when the orbital separation is approximately one-tenth of its initial value and the red giant envelope is already aspherical which is consistent with our prescription. Most of the mass loss ( $\sim 0.3M_{\text{env}}$ ) is concentrated in the equatorial plane in this more energetic case. The equivalent energy parameter is  $\alpha = \Delta E/E_B \approx 1.2$  whereas we consider the range  $\alpha = 0.25\text{--}0.5$ .

## 4 APPLICATIONS TO SN 1987A AND SHERIDAN 25

Many non-spherical nebulae are axially symmetric, which has been interpreted as evidence for rapid rotation, possibly as a result of binary interactions. A notable example is the mysterious nebula surrounding the supernova SN 1987A, which consists of three roughly parallel rings, one centred on the supernova and the other two displaced by  $\sim 1$  arcsec to either side (Burrows et al. 1995). The supernova itself was anomalous in several other respects (see Podsiadlowski 1992, and references therein), which are most consistent with a binary merger some 20 000 yr before the supernova event (Podsiadlowski 1992; Podsiadlowski & Ivanova 2003). In particular, the blue supergiant progenitor and the chemical anomalies in the inner ring can easily be explained as the result of the

**Table 4.** Observed properties of circumstellar material around massive stars. Bracketed periods denote systems which are too wide to undergo binary interactions. The properties of the material in the equatorial torus are given in the last four columns, where  $R$ ,  $v$  and  $t$  give the radius, expansion velocity and dynamical age, respectively.

Star	Spectral type	Period	Luminosity $L/L_{\odot}$	Density ( $\text{cm}^{-3}$ ) or mass	Equatorial torus $R$ ( $10^{17}$ cm)	$v$ ( $\text{km s}^{-1}$ )	$t$ (yr)
Sk $-69^{\circ}$ 202	B3 Ia	–	$10^{5.2}$	$n_e \sim 2\text{--}5 \times 10^4$	$6.23 \pm 0.08^a$	10.3	19 000
Sheridan 25	B1.5 Iab	–	$10^{5.9}$	$0.01\text{--}0.1 M_{\odot}$	6.2	20	6600
RY Scuti	O6.5 + O9.5 <sup>b</sup>	11.3 d	$\sim 10^6$	$1 M_{\odot}?$	0.2	50	130
$\eta$ Carinae	? Ia	(5.5 yr)	$10^{6.7}$	$3\text{--}15 M_{\odot}^c$	0.7	50	$\sim 1000$
R4 <sup>d</sup>	B[e] + A	(21.3 yr)	$10^5 + 10^{4.2}$	?	?	?	$\sim 10\,000$

Note. Data taken from <sup>a</sup>Panagia (2004), <sup>b</sup>Smith et al. (2001), <sup>c</sup>Morris et al. (1999), Smith et al. (2003) and <sup>d</sup>Zickgraf et al. (1996).

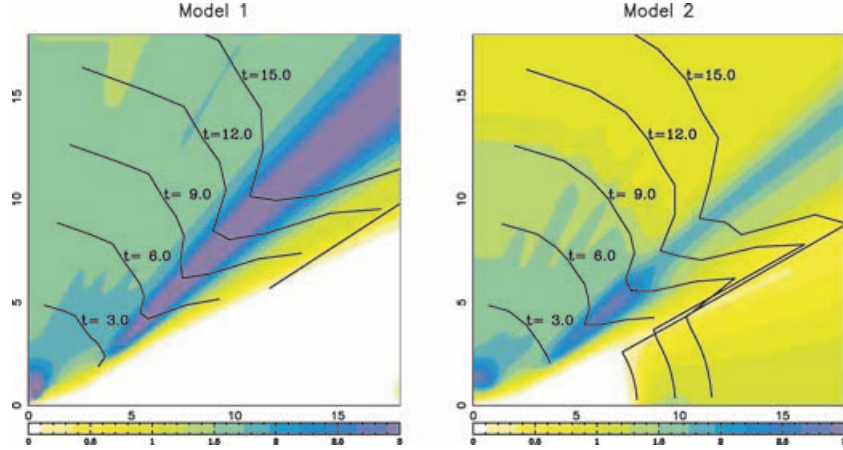


**Figure 10.** Mass enhancements in the ejecta flow, corresponding to merger models for SN 1987A (left-hand panel; Model 1 from Section 3.1 with  $\alpha = 0.33$  and  $\beta = 0.817$ ) and Sheridan 25 (right-hand panel; Model 2 from Section 3.2 with  $\alpha = 0.35$  and  $\beta = 0.665$ ). The solid curves give the location that contains 50 per cent of the mass ejected at a particular solid angle at the time as indicated (in code units).

dredge-up of core material in the final stage of the merger (Ivanova & Podsiadlowski 2003).

The fast wind ( $\dot{M} \sim 10^{-7} M_{\odot} \text{ yr}^{-1}$ ,  $v_{\infty} \sim 500 \text{ km s}^{-1}$ ) of such a blue supergiant will sweep up and enhance any structures already present in the ejecta, leading to an axially symmetric but highly aspherical nebula.

#### 4.1 Late Case B/C merger: SN 1987A

During late He-shell burning the primary will be a red supergiant with a critical surface rotation velocity of

$$v_{\text{cr}} \sim 45 \text{ km s}^{-1} \left( \frac{M}{15 M_{\odot}} \frac{1500 R_{\odot}}{R} \right)^{1/2} \quad (9)$$

which is comparable to the velocities observed in the SN 1987A nebula (see Table 4). The latitude dependence of the ejected material of Model 1, shown in Fig. 10, is characterized by a strong enhancement at mid-latitudes, while no material is lost in the equatorial region. The following features of the nebula may therefore be understood.

(i) *Strong mass enhancement in the outer rings (ORs).* The ORs are a real density enhancement (100 times the ambient value) and are not simply due to limb brightening of an hourglass structure (Burrows et al. 1995). In our model the ORs result from wind-driven pressure gradients in the seed structures which directly result from the anisotropic ejection of material during the merger phase. Previous models based only on equatorial density enhancements

in the pre-existing material have been unable to explain the high density in the ORs (e.g. Martin & Arnett 1995).

(ii) *Displacement of the ORs relative to the inner ring.* We favour a model in which the inner ring originates a few 1000 yr after the merger event, in a rotation-enforced outflow during contraction on the post-merger blue loop (Heger & Langer 1998; also see Collins et al. 1999). The relative displacement of the ORs can be understood if the mass ejection during the merger event itself was slightly asymmetric, perhaps due to a non-axisymmetric pulsational instability in the envelope, which gives the ejecta a velocity of  $\sim 2 \text{ km s}^{-1}$  relative to the merger remnant. Hence, the wind-driven pressure gradients are no longer axisymmetric and the planes<sup>2</sup> in which the ORs lie will be slightly inclined with respect to the plane of the inner ring. This would explain both the offset of the ORs and their shape, which is notably non-elliptical in projection.

(iii) *North–south asymmetry.* Since the planes of the ORs are no longer parallel to one another, the Southern OR is observed closer to face-on in projection than the Northern one.

#### 4.2 Case B merger: Sheridan 25

Mass loss during CE evolution may explain the broadly similar structures seen around other luminous stars, listed in Table 4. Of these, the nebula around the B1.5 supergiant Sheridan 25 shows the most compelling similarities, since it has an equatorial ring

<sup>2</sup> The ORs are still approximately planar in this case.

of at least  $0.01\text{--}0.10 M_{\odot}$  (Brandner et al. 1997b) and polar lobes, each containing  $\sim 0.25 M_{\odot}$ . It is in a post main sequence, though probably pre-red supergiant, evolutionary state (with  $N/C \sim 26$ ,  $N/O = 0.36$ , Smartt et al. 2002). The dynamical age of the nebula has been estimated to be around 6000 yr. The observed velocities suggest an envelope radius of  $\sim 300 R_{\odot}$  at the time of ejection, corresponding to a merger during the Hertzsprung-gap crossing.

Although the density structure of the CE will differ from that of a  $\gamma = 5/3$  condensed polytrope, the results may still be applicable if the envelope is aspherical. We suggest a model with equatorial mass loss during the merger, such as Model 2 discussed above (see right-hand panel of Fig. 10), since the envelope cannot store enough angular momentum to generate a significant post-merger equatorial outflow. Hence, an asymmetry during the merger will displace both the equatorial and polar material from the site of the merged star. The equatorial ring is offset from Sheridan 25 by  $0.05\text{--}0.1$  pc (Brandner et al. 1997a), which is consistent with this model.

### 4.3 Conclusions

The three principal anomalous features of the supernova SN 1987A, viz. its blue supergiant progenitor, its over-abundance of certain elements, notably He, and the presence of highly structured circumstellar material, are all consistent with a binary merger some 20 000 yr before the explosion. In this paper, we have demonstrated how density enhancements at mid-latitudes arise during mass ejection from a rotationally distorted star. Subsequent interaction with the fast wind of the blue supergiant prior to the supernova (cf. Blondin & Lundqvist 1993) then leads to the formation of the ORs with a density enhancement of a factor of 150, in calculations of Morris & Podsiadlowski (2005) which will be further discussed in a future paper.

Similarly, the nebula around Sheridan 25 may be explained by a binary merger following a CE phase during the crossing of the Hertzsprung gap by the primary. One notable difference in this case is that the equatorial ring likely originates during the merger, which is consistent with observations showing that the centre of the equatorial ring is displaced by some 0.05 pc from Sheridan 25. Future observations of the rotation rate of Sheridan 25 would help to confirm this model.

Although the nebula around the more massive system RY Scuti (O9.5 + O6.5) appears similar, its evolution is probably somewhat different. Data from the Keck telescope and the *Hubble Space Telescope*, discussed in Smith et al. (1999) and Smith, Gerhz & Goss (2001), show a massive equatorial dust torus and two narrow rings symmetrical about the equatorial plane, with a dynamical age of 120 yr. The massive torus probably originated during thermal time-scale mass outflow from the outer Lagrangian L2 point which is still occurring today, albeit at the much lower rate of  $\sim 5 \times 10^{-5} M_{\odot} \text{ yr}^{-1}$ . Subsequent deflection of the fast wind in a manner somewhat analogous to the horseshoe model of Soker (1999) may explain the origin of the two narrow rings.

Pasquali et al. (2000) have suggested that the B[e] component of the spectroscopic binary R4 in the Large Magellanic Cloud (LMC) could be the result of a Case B/C merger, that is, the system would originally have been a triple system, where the companion A star now serves as an astronomical clock and indicates that the present primary has lost  $\gtrsim 40$  per cent of its zero-age main-sequence (ZAMS) mass (Zickgraf et al. 1996). Since the companion is already a post-main sequence A supergiant, the pre-merger components cannot be much more massive, for example,  $12\text{--}15 M_{\odot}$  for the original primary. In addition, Pasquali et al. (2000) find evidence of CNO-

processed circumstellar material with a dynamical age of  $\sim 10^4$  yr which is consistent with ejection during a binary merger. Direct images of the nebula would be of great benefit to understanding this system.

Bipolarity is also common in observations of planetary nebulae. Asymmetric mass loss during a CE phase (with or without a merger) provides physical motivation for the equatorial density enhancement functions proposed by Icke, Balick & Preston (1999) and Luo & McCray (1991) (see also Frank 1999). We speculate that the homunculus nebula around  $\eta$  Carinae may also have originated during a CE phase since its kinetic energy is  $\sim 10^{50}$  erg (Smith et al. 2003a), comparable to the luminous energy of the 1840–1860 outburst. Both the mass-loss rate in the stellar wind ( $1.6 \times 10^{-3} M_{\odot} \text{ yr}^{-1}$ ) and its latitude dependence suggest rapid rotation of the central star (Smith et al. 2003b; van Boekel et al. 2003; Aerts et al. 2004). In the merger scenario  $\eta$  Carinae was originally a triple system in which the closer components ( $P \sim 30$  d) merged 150 yr ago to leave the present companion in an eccentric 5.5-yr orbit.

### ACKNOWLEDGMENTS

The computations reported here were performed using the UK Astrophysical Fluids Facility (UKAFF). The authors would also like to thank N. Langer for stimulating discussions.

### REFERENCES

- Aerts C., Lamers H. J. G. L. M., Molenbergh G., 2004, *A&A*, 418, 639  
 Bjorkman J. E., Cassinelli J. P., 1993, *ApJ*, 409, 429  
 Blondin J., Lundqvist P., 1993, *ApJ*, 405, 337  
 Bodenheimer P., Ostriker J. P., 1973, *ApJ*, 180, 159  
 Brandner W., Grebel E. K., Chu Y.-H., Weis K., 1997a, *ApJ*, 475, L45  
 Brandner W., Chu Y.-H., Eisenhauer F., Grebel E. K., Points S. D., 1997b, *ApJ*, 489, L153  
 Burrows C. et al., 1995, *ApJ*, 452, 680  
 Collins T. J. B., Frank A., Bjorkman J., Livio M., 1999, *ApJ*, 512, 322  
 Frank A., 1999, *New Astron. Rev.*, 43, 31  
 Heger A., Langer N., 1998, *A&A*, 334, 210  
 Icke V., Balick B., Preston H., 1989, *AJ*, 97, 462  
 Ivanova N., Podsiadlowski Ph., 2003, in Hillebrandt W., Leibundgut B., eds, *From Twilight to Highlight: The Physics of Supernovae*. Springer, Berlin, p. 19  
 Livio M., Soker N., 1988, *ApJ*, 329, 764  
 Lucy L. B., 1977, *AJ*, 82, 1013  
 Luo D., McCray R., 1991, *ApJ*, 379, 659  
 Martin C. L., Arnett D., 1995, *ApJ*, 447, 378  
 Meyer F., Meyer-Hofmeister E., 1979, *A&A*, 78, 167  
 Monaghan J. J., 1992, *ARA&A*, 30, 543  
 Morris P. W. et al., 1999, *Nat*, 402, 502  
 Morris T., Podsiadlowski Ph., 2005, in Turratto M., ed, 1604–2004: Supernovae as Cosmological Lighthouses. Astron. Soc. Pac., San Francisco  
 Paczyński B., 1976, in Eggleton P., Mitton S., Whelan J., eds, *Structure and Evolution of Close Binary Systems*. Reidel Publishing Co., Dordrecht, p. 75  
 Panagia N., 2004, in Marcaide J. M., Weiler K. W., eds, *Supernovae: Ten Years of SN1993J*. Springer, Berlin, p. 585  
 Pasquali A., Nota A., Langer N., Schulte-Ladbeck R. E., Clampin M., 2000, *AJ*, 119, 1352  
 Podsiadlowski Ph., 1992, *PASP*, 104, 717  
 Podsiadlowski Ph., 2001, in Podsiadlowski Ph., Rappaport S., King A. R., D'Antona F., Burderi L., eds, *Evolution of Binary and Multiple Star Systems*. ASP, San Francisco, p. 239  
 Podsiadlowski Ph., Ivanova N., 2003, in Hillebrandt W., Leibundgut B., eds, *From Twilight to Highlight: The Physics of Supernovae*. Springer, Berlin, p. 13

- Pols O. R., 1994, *A&A*, 290, 119  
 Sandquist E. L. et al., 1998, *ApJ*, 500, 909  
 Smartt S. J., Lennon D. J., Kudritzki R. P., Rosales F., Ryans R. S. I., Wright N., 2002, *A&A*, 391, 979  
 Smith N., Gerhz R. D., Humphreys R. M., Davidson K., Jones T. J., Krautter J., 1999, *AJ*, 118, 960  
 Smith N., Gerhz R. D., Goss W. M., 2001, *AJ*, 122, 2700  
 Smith N., Gerhz R. D., Hinz P. M., Hoffmann W. F., Hora J. L., Mamajek E. E., Meyer M. R., 2003a, *AJ*, 125, 1458  
 Smith N., Davidson K., Gull T. R., Ishibashi K., Hillier D. J., 2003b, *ApJ*, 586, 432  
 Soker N., 1999, *MNRAS*, 303, 611  
 Springel V., Yoshida N., White S. D. M., 2001, *New Astron.*, 6, 51  
 Taam R. E., Sandquist E. L., 2000, *ARA&A*, 38, 113  
 van Boekel R. et al., 2003, *A&A*, 410, 37  
 Wellstein S., Langer N., Braun H., 2001, *A&A*, 369, 939  
 Zickgraf F.-J., Kovacs J., Wolf B., Stahl O., Kaufer A., Appenzeller I., 1996, *A&A*, 309, 505

## APPENDIX A: RESOLUTION STUDY

Fig. A1 shows that increasing the number of particles by a factor of 2 does not significantly change the geometry of the ejecta. This implies

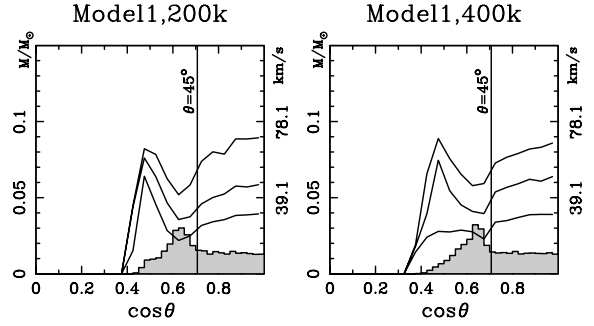


**Figure A1.** Comparison between two calculations of Model 1, with  $2 \times 10^5$  particles (left-hand panel) and  $4 \times 10^5$  particles (right-hand panel).

that our calculations have converged numerically. The calculation is limited by the physical approximations such as the assumption of a polytropic equation of state.

This paper has been typeset from a  $\text{\TeX}/\text{\LaTeX}$  file prepared by the author.